Supporting Information

Ultrastable Hydrated Vanadium Dioxide Cathodes for High-Performance Aqueous Zinc Ion Batteries with H^+/Zn^{2+} Co-insertion Mechanism

Xiudong Chen,[a,b,‡,*] Xiesen Hu,[b,‡] Yaoyao Chen,[b] Xiaohua Cao,[a,*] Yan Huang,[b,*] Hang Zhang,[c] Jin-Hang Liu,[a] Yawei Wang,[a] Shu-Lei Chou,[c,*] and Dapeng Cao[b,*]

[a] *School of Chemistry and Chemical Engineering, Jiangxi Province Engineering Research Center of Ecological Chemical Industry, Jiujiang University, Jiujiang 332005, China*

E-mail: chenxd@jju.edu.cn,caojimmy@126.com

[b] *State Key Laboratory of Organic-Inorganic Composites, Beijing University of Chemical Technology, Beijing 100029, China*

E-mail: huangyan@mail.buct.edu.cn, caodp@mail.buct.edu.cn

[c] *Institute of Carbon Neutralization College of Chemistry and Materials Engineering, Wenzhou University, Wenzhou 325035, China*

E-mail: chou@wzu.edu.cn

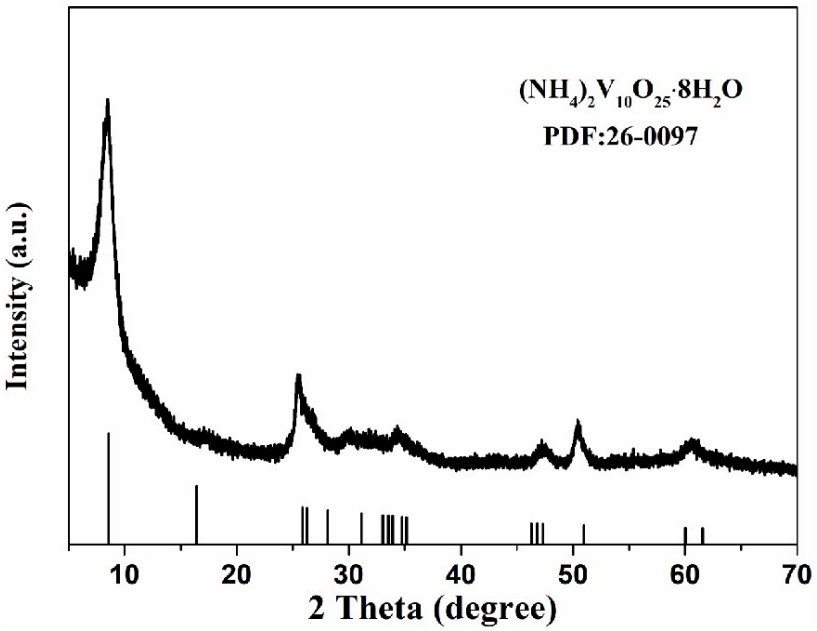

Fig. S1 XRD pattern of $(NH_4)_2V_{10}O_{25}\cdot 8H_2O$.

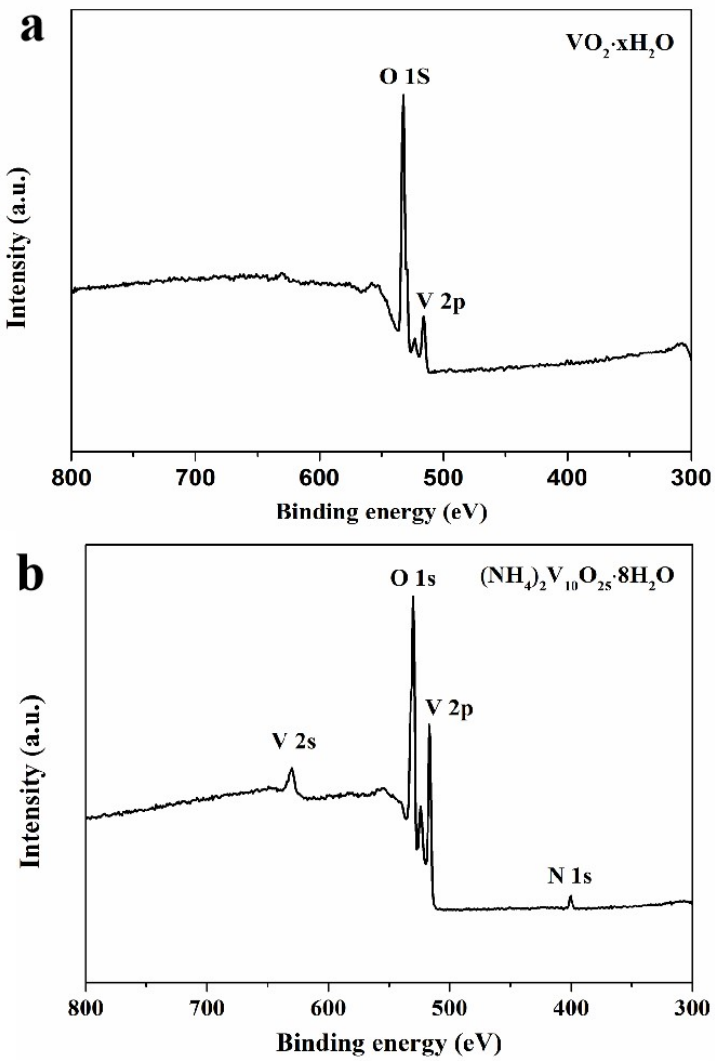

Fig. S2 XPS full spectra of a) $VO_2 \cdot xH_2O$ and b) $(NH_4)_2V_{10}O_{25} \cdot 8H_2O$.

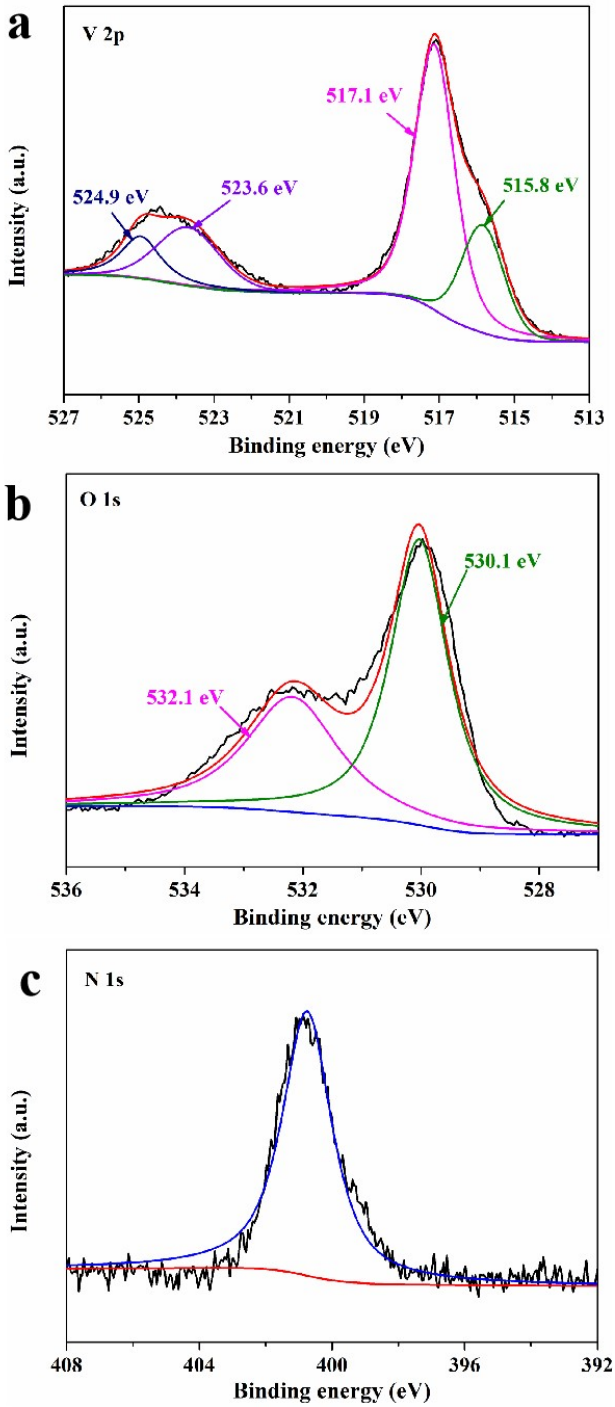

Fig. S3 XPS spectrum of the $(NH_4)_2V_{10}O_{25}\cdot 8H_2O$ corresponding high resolution XPS spectra of a) V 2p, b) O 1s, and c) N 1s.

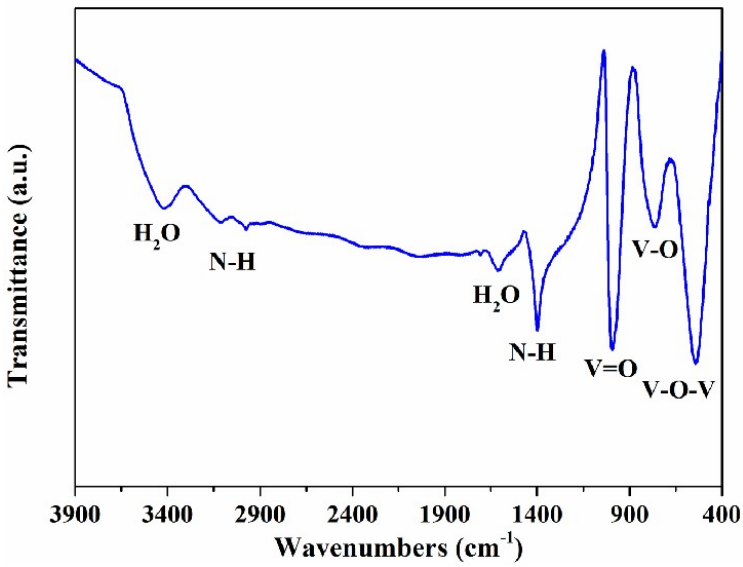

Fig. S4 FTIR spectrum of the $(NH_4)_2V_{10}O_{25}\cdot 8H_2O$.

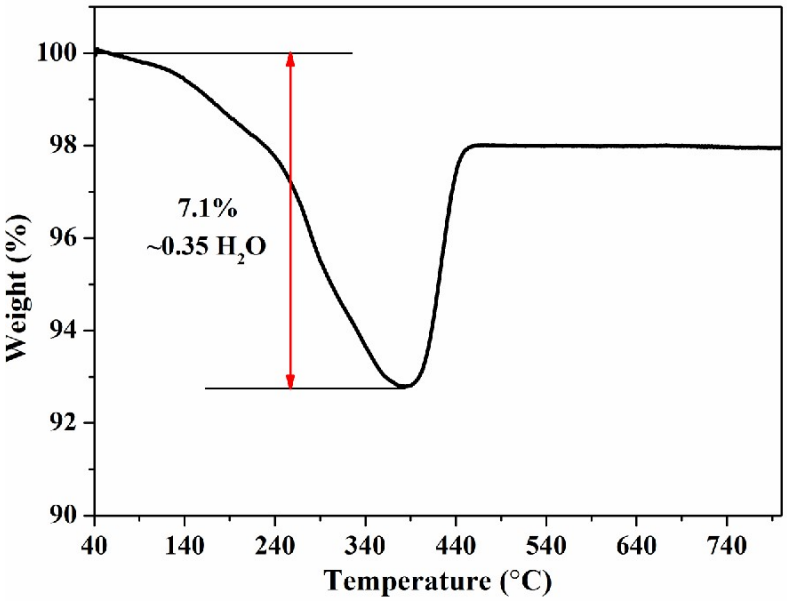

Fig. S5 TGA curve of the $VO_2 \cdot xH_2O$ under O_2 atmosphere.

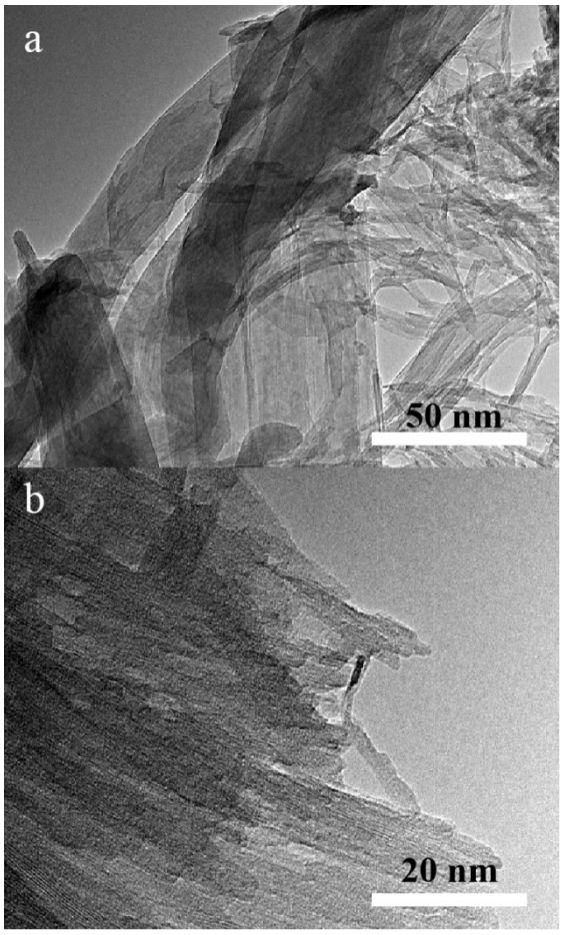

Fig. S6 HRTEM images of the $(NH_4)_2V_{10}O_{25}\cdot 8H_2O$

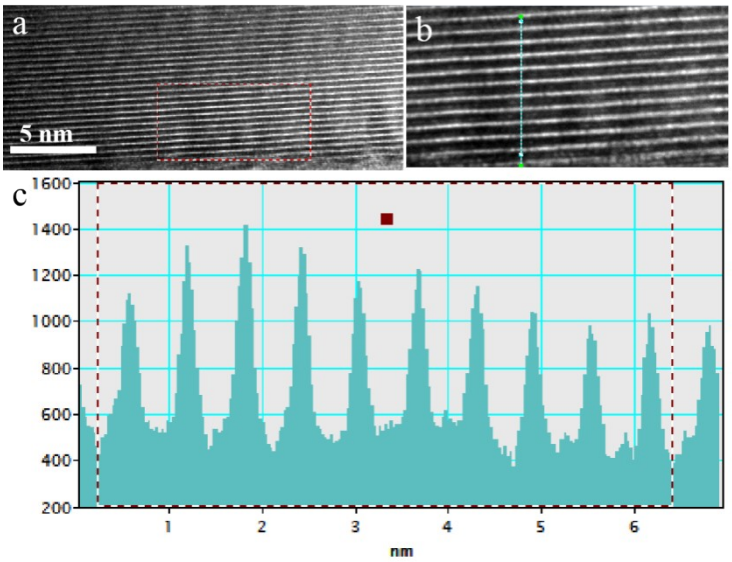

Fig. S7 The lattice spacing determination of $VO_2 \cdot xH_2O$: a) HRTEM image, b) lattice fringes of HRTEM image, c) the lattice spacing (~0.62nm) of ten lattice fringes. In order to calculate the change of d value during cycling, ten lattice fringes were measured.

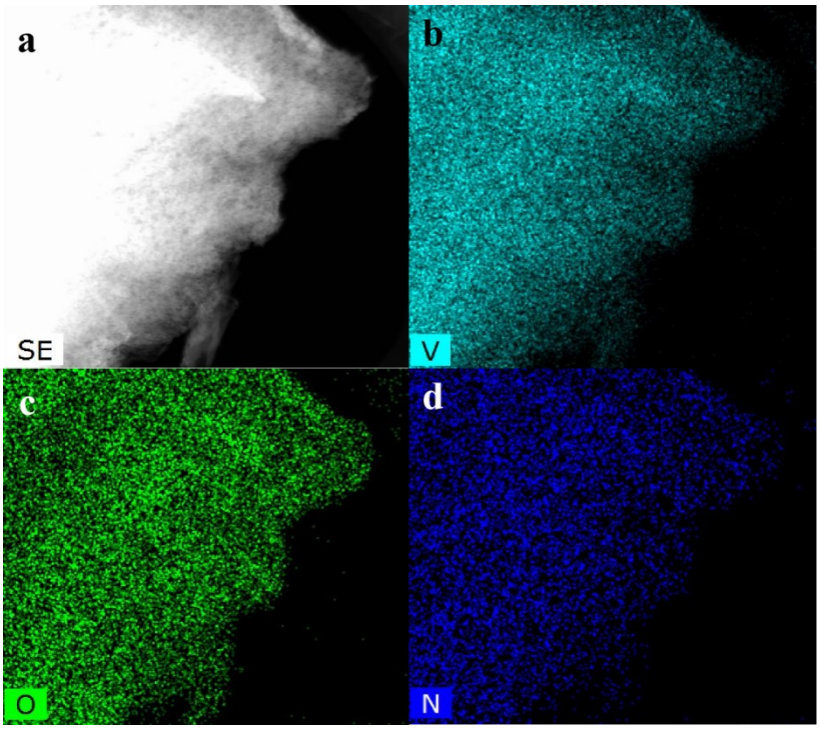

Fig. S8 HAADF-STEM images with EDS mapping of the $(NH_4)_2V_{10}O_{25}\cdot 8H_2O$.

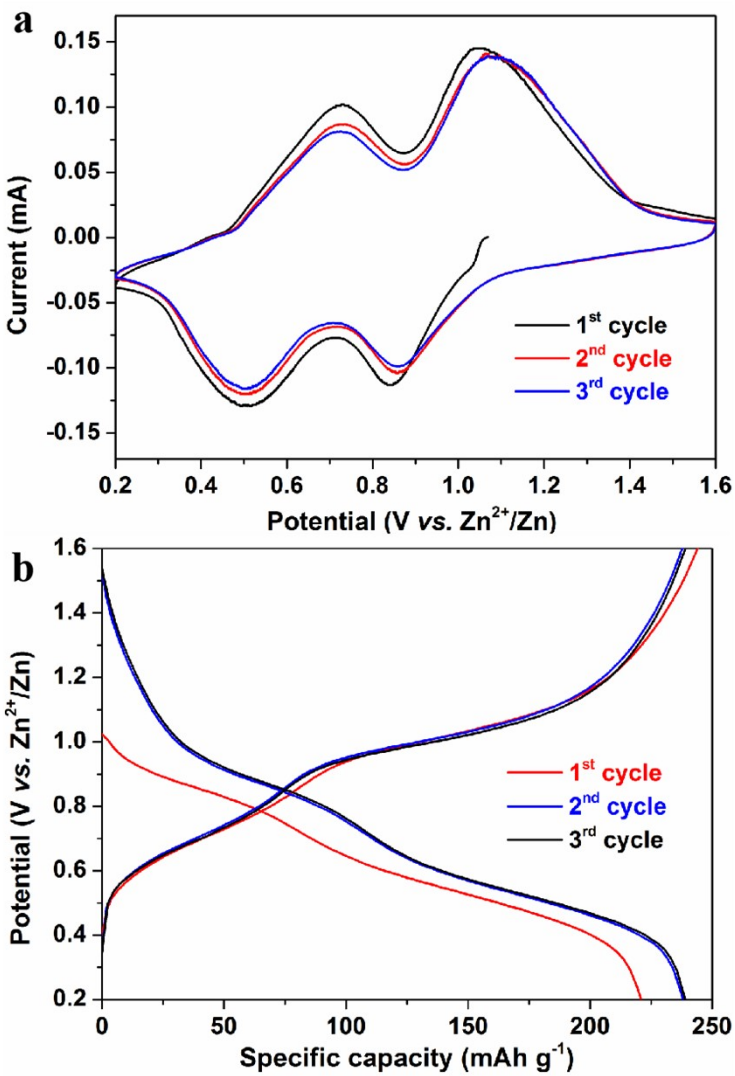

Fig. S9 a) The CV curves of $(NH_4)_2V_{10}O_{25}\cdot 8H_2O$ at 0.1 mV s^{-1}. b) Charge- discharge curves of $(NH_4)_2V_{10}O_{25}\cdot 8H_2O$ for the first three cycle at 1 A g^{-1}.

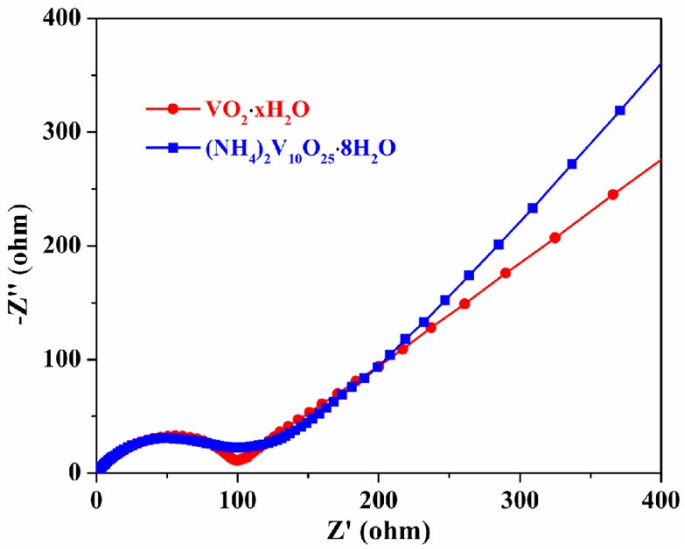

Fig. S10 The Nyquist plots for $VO_2 \cdot xH_2O$ and $(NH_4)_2V_{10}O_{25} \cdot 8H_2O$ cathode after the first cycles

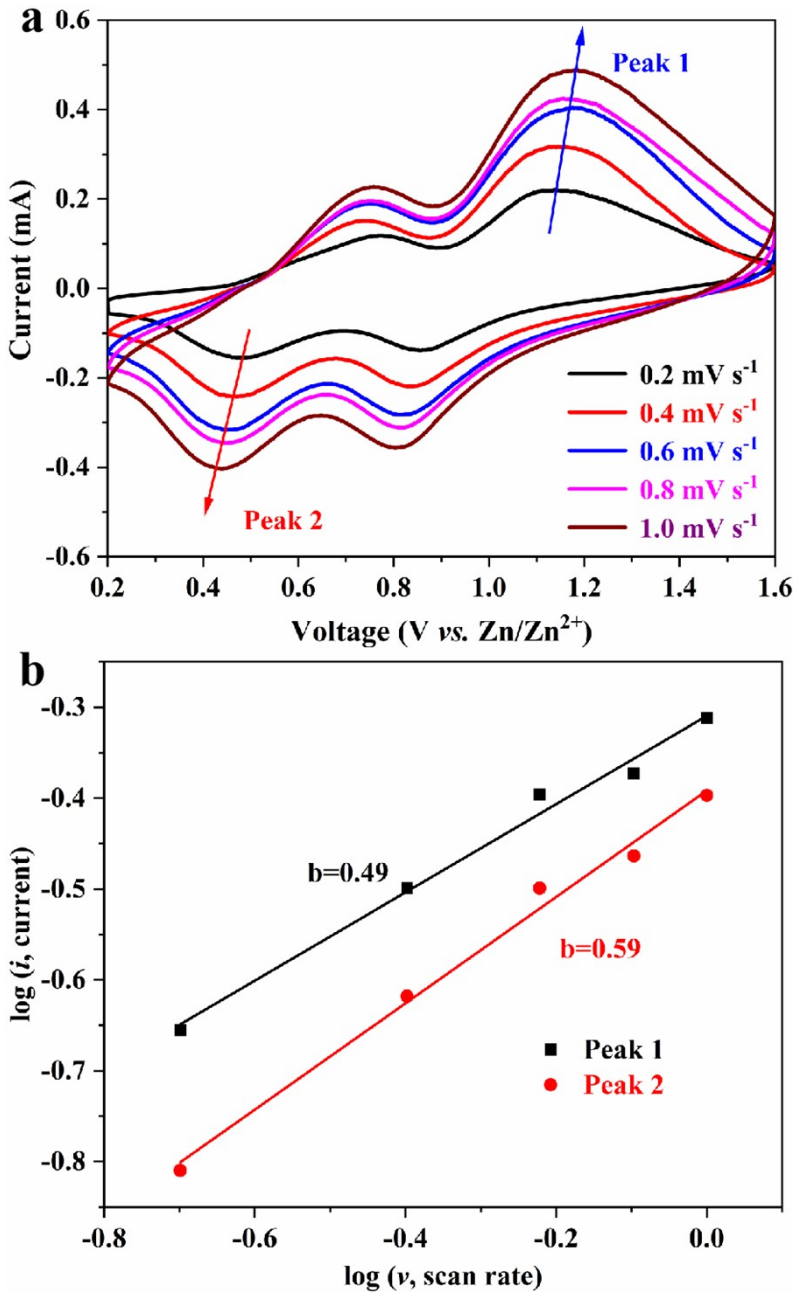

Fig. S11 a) CV curves of $(NH_4)_2V_{10}O_{25}\cdot 8H_2O$ in 2 M $Zn(CF_3SO_3)_2$ electrolyte at various scan rates from 0.2 to 1.0 mVs^{-1}. b) log(i) versus log(v) curves of cathodic and anodic peak.

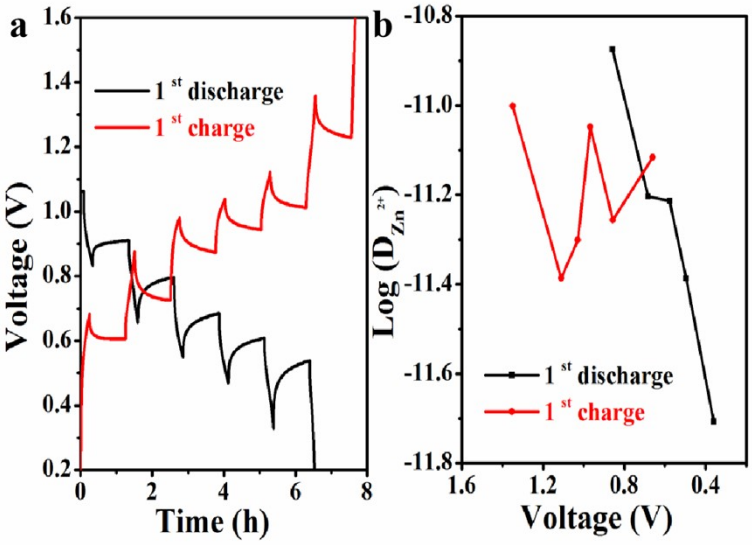

Fig. S12 a) Discharge and charge GITT profile of $(NH_4)_2V_{10}O_{25}\cdot 8H_2O$ for the first cycle. b) Diffusivity coefficient at different discharge and charge states during GITT measurement.

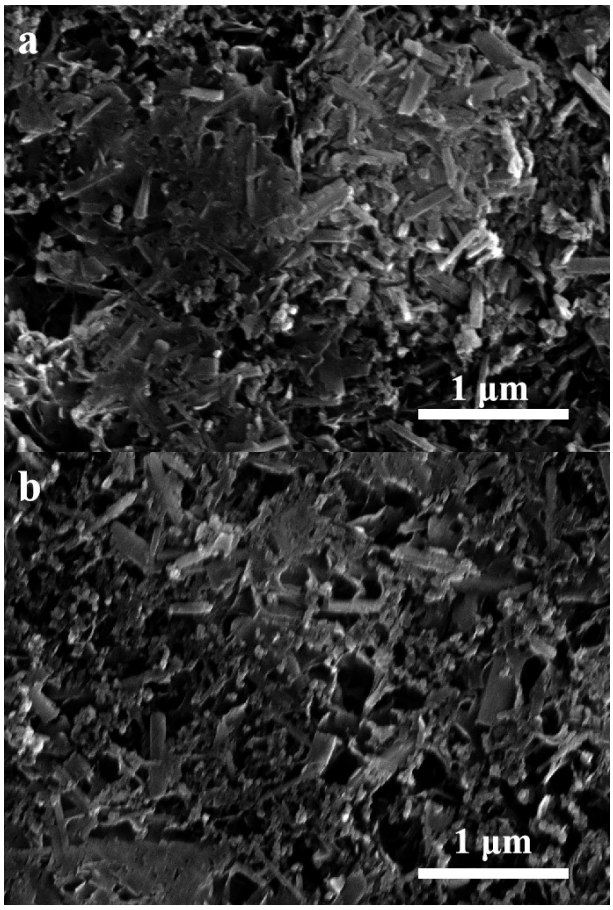

Fig. S13 FESEM images of the holey $VO_2 \cdot xH_2O$ electrode at various cycled states: a) fully discharged to 0.2 V and b) fully charged to 1.6 V in the first cycle.

Table S1. Detailed structural information on the $VO_2 \cdot xH_2O$ sample after Rietveld refinement.

Monoclinic, space group *C2/m(12)*, a=6.296112 Å, b=6.297671 Å, c=6.427364 Å, α=73.845°, β=73.817°, γ=34.114°, V=136.732 Å^3, R_{wp}=5.25%, R_p=3.97%.

atom	x	y	z	Occ.	U
V0	0.29822	0.30782	0.26806	1	0.01
V1	0.69665	0.69507	0.72462	1	0.01
V2	0.3988	0.3988	0.68529	1	0.01
V3	0.6012	0.6012	0.31471	1	0.01
O4	0.33141	0.39982	0.00623	1	0.01
O5	0.64554	0.63362	0.99449	1	0.01
O6	0.23787	0.23787	0.64901	1	0.01
O7	0.76213	0.76213	0.35099	1	0.01
O8	0.46035	0.46558	0.30358	1	0.01
O9	0.55199	0.57209	0.63651	1	0.01
O10	0.14904	0.09801	0.29463	1	0.01
O11	0.86531	0.86531	0.70082	1	0.01

Table S2. Electrochemical properties compared between $VO_2 \cdot xH_2O$ and previously reported VO_2 materials (IRC: initial reversible capacity, mAh g^{-1}; RRC: retained reversible capacity, mAh g^{-1}; CN: cycle number; CD: current density, A g^{-1}).

Composite	IRC	RRC	CN	CD	Reference
$VO_2 \cdot xH_2O$	302	376	1	200	This work
	283	289	5	2000	
	197	206	15	8000	
holey C@VO_2	386.9	345.8	0.2	100	1
	332	280	5	600	
RGO/VO_2	242	240	1	1000	2
VO_2(B)/RGO	~240	216	5	1600	3
VO_2	~160	~220	0.5	350	4
	~105	~100	5	10000	
nsutite-type VO_2	314.4	310	1	100	5
	50	163.5	5	5000	
Na^+ doping VO_2	397	301	0.2	110	6
	156	118	12	3000	
VO_2@NC	269.3	268.5	10	2500	7
$VO_2 \cdot 0.45H_2O$	200	140	5	3000	8
β-VO_2/CNTs	205	165	3	5000	9

References:

1 M. Yang, D. Ma, H. Mi, X. Yang, Y. Wang, L. Sun and P. Zhang, A unique morphology and interface dualengineering strategy enables the holey C@VO_2 cathode with enhanced storage kinetics for aqueous Zn-ion batteries, *J. Mater. Chem. A* 2021, **9**, 8792-8804.

2 X. Dai, F. Wan, L. L. Zhang, H. M. Cao and Z. Q. Niu, Freestanding graphene/VO_2 composite films for highly stable aqueous Zn-ion batteries with superior rate performance, *Energy Storage Mater.* 2019, **17**, 143-150.

3 F. Cui, J. Zhao, D. Zhang, Y. Fang, F. Hu and K. Zhu, VO_2(B) nanobelts and reduced graphene oxides composites as cathode materials for low-cost rechargeable aqueous zinc ion batteries, *Chem. Eng. J.* 2020, **390**, 124118.

4 T. Y. Wei, Q. Li, G. Z. Yang and C. X. Wang, An electrochemically induced bilayered structure facilitates long-life zinc storage of vanadium dioxide, *J. Mater. Chem. A* 2018, **6** , 8006-8012.

5 Y.-Y. Liu, T.-T. Lv, H. Wang, X.-T. Guo, C.-S. Liu and H. Pang, Nsutite-type VO_2 microcrystals as highly durable cathode materials for aqueous zinc-Ion batteries, *Chem. Eng. J.* 2021, **417**, 128408.
6 Y. Liu and X. Wu, Hydrogen and sodium ions co-intercalated vanadium dioxide electrode materials with enhanced zinc ion storage capacity, *Nano Energy* 2021, **86**, 106124.
7 T.-T. Lv, X. Luo, G.-Q. Yuan, S.-Y. Yang and H. Pang, Layered VO_2@N-doped carbon composites for high-performance rechargeable aqueous zinc-ion batteries, *Chem. Eng. J.* 2022, **428**, 131211.
8 K. Zhu, T. Wu, S. Sun, W. van den Bergh, M. Stefik and K. Huang, Synergistic H^+/Zn^{2+} dual ion insertion mechanism in high-capacity and ultra-stable hydrated VO_2 cathode for aqueous Zn-ion batteries, *Energy Storage Mater.* 2020, **29**, 60-70.
9 X. Fan, X. Wen, Y. Tang, W. Zhou, K. Xiang and H. Chen, β-VO_2/carbon nanotubes core-shelled microspheres and their applications for advanced cathode in aqueous zinc ion batteries, *Electrochim. Acta* 2021, **400**, 139425.